International Journal of Information, Control and Computer Sciences
ISSN: 2517-9942
Vol:5, No:3, 2011

Stochastic Modeling and Combined Spatial Pattern Analysis of Epidemic Spreading

S. Chadsuthi, W. Triampo, C. Modchang, P. Kanthang, D. Triampo, N. Nuttavut

***Abstract*—**We present analysis of spatial patterns of generic disease spread simulated by a stochastic long-range correlation SIR model, where individuals can be infected at long distance in a power law distribution. We integrated various tools, namely perimeter, circularity, fractal dimension, and aggregation index to characterize and investigate spatial pattern formations. Our primary goal was to understand for a given model of interest which tool has an advantage over the other and to what extent. We found that perimeter and circularity give information only for a case of strong correlation—while the fractal dimension and aggregation index exhibit the growth rule of pattern formation, depending on the degree of the correlation exponent (β). The aggregation index method used as an alternative method to describe the degree of pathogenic ratio (α). This study may provide a useful approach to characterize and analyze the pattern formation of epidemic spreading

***Keywords*—**spatial pattern epidemics, aggregation index, fractal dimension, stochastic, long-rang epidemics

I. Introduction

PATTERN formation phenomena, occurring via the aggregation process or clustering of particles, has been the subject of increased interest [1]. Spatial pattern analysis plays an important role in many fields of research, ranging from the microscopic to macroscopic scale, including bacteria colonies [2], epidemiology [3], forests, and ecology [4]. Spatial technology enables epidemiologists to create detailed maps and employ spatial cluster statistics to garner insights about patterns of disease [3]. There has been significant development in creating predictive models to better understand the pattern formation of epidemics; see reviews [5-7]. The mathematical epidemiological model usually takes the form of a deterministic model, which consists of a system of ordinary differential equation (ODE) models describing changes in the number of susceptible, infected, and recovered individuals in a given population [8]. Typically, the ODE deterministic model neglects spatial correlation by assuming that the system is spatially homogeneous; this is also termed the mean field approximation approach [9]. In addition, the ODE deterministic model can exactly determine the transient evolution of the system once the initial condition is given. However, for epidemical phenomena where there is a large degree of spatial organization or pattern formation of spreading, the ODE deterministic model may be unrealistic.

It is important to account for spatial variation and to study the landscape as well as the pattern formations of epidemic phenomena. With regard to spatial pattern driven forces such as diffusion, deterministic partial differential equation (PDE) models are well known conventional tools for analyzing dynamical aspects [10], but such models do not take into account the noises or stochastic fluctuations associated with spatiotemporal dynamics. Consequently, stochastic partial differential equation (SPDE) models, such as the Langevin equation, are needed [11]. However, it usually is difficult to obtain analytical solutions to compare with experimental data. Therefore, computer simulations can be of great help in investigating spatial patterns that are typically due to the effect of noise. One of the most efficient is the Monte Carlo based spatial cellular automata model.

In our current work, we were interested in studying the spatial pattern formation of epidemic spreading using the Monte Carlo simulation approach. Even though the model of interest is generic; we believe that our findings could be useful in understanding how diseases spread, and how to prevent epidemic spreading.

To characterize the spatial pattern of epidemics, there are many parameters that can be used to analyze the patterns—for example, area, perimeter [12], circularity [12, 13], fractal dimension [14], and aggregation index [15]. These parameters provide different information at least to some extent. Area and perimeter measurements are very familiar and straight forward to understand. More interesting is circularity, which is a numerical quantity representing the degree to which a shape is compact. It is calculated from the perimeter, which is defined as a path surrounding an area. This measurement of a region is a common technique used to characterize pattern patchiness and compactness [12]. Topologically, the circularity value should be invariant under similarity transformations of the shape, such as scaling, rotation and translation. However this measurement can be used to describe the interaction between individuals.

Fractal dimension (D_f) can be defined as a measure of structural complexity [1]. It has attracted considerable attention from many mathematicians because its fractional quality is in sharp contrast to the integer dimensions (zero, one, two, and three) of Euclidean geometry. It is an index used to indicate how completely a fractal appears to fill spaces, as

S. Chadsuthi, C. Modchang and N. Nuttavut are with Biophysics Group, Department of Physics, Faculty of Science, Mahidol University, Rama VI, Ratchathewi District, Bangkok Thailand 10400

W. Triampo is with Biophysics Group, Department of Physics, Faculty of Science, Mahidol University, Rama VI, Ratchathewi District, Bangkok Thailand 10400, ThEP Center, CHE, 328 Si Ayutthaya Road, Bangkok, Thailand 10400, Institute for Innovative Learning, Mahidol University, 999, Phuttamonthon 4 Road, Salaya, Nakorn Pathom 73170, Thailand (corresponding author to provide phone: +662-441-9816 ext. 1131; fax +662-441-9322; e-mail wtriampo@gmail.com, scwtr@mahidol.ac.th)

P. Kanthang is with Department of Physics, Facutly of Science and Technology, Rajamangala University of Technology, Phra Nakhon, Bangkok Thailand 10800

D. Triampo is with Department of Chemistry, Center of Excellence for Innovation in Chemistry, Faculty of Science, Mahidol University, Rama VI, Ratchathewi District, Bangkok, Thailand 10400

one zooms down to finer and finer scales. The term fractal is used to describe fractured shapes, which possess repeating patterns when viewed at magnified resolution. This special value of scale invariance, which shows up in many natural patterns, can be identified and quantified by a parameter called the fractal dimension [16]. Lastly, an aggregation index (*AI*), which is used to represent the quantitative measurement of aggregation levels of spatial patterns, is class specific and independent of landscape composition [15]. Characteristically, the AI is used to describe the level of aggregation by considering adjacent matrixes or the contact perimeters. From our review, most published research works solely apply one or at most two parameters in characterizing the spatial pattern of epidemic spreading [17-19]. For example, Tan and co-workers used only the fractal dimension to investigate epidemic spreading [18]. Likewise, Hagerhall and co-worker used only the fractal dimension with empirical evidence in seeking connections between landscape preferences [16]. In our opinion, multi-quantifications tend to provide better insight into the problems associated with the dynamics of the epidemic process. To our knowledge no (or very few) researchers have used the aggregation index to indicate the aggregation level for epidemic spreading. Hence in our work, we applied various quantitative spatial characterizations to analyze the spatial pattern of a spreading epidemic. These include: perimeter, circularity, fractal dimension, and aggregation index. Our primary goals were to provide the information obtained by each of these measurements; characterize the most effective measurement; describe the advantages or disadvantages associated with each measurement; and establish how many parameters need to be combined in order to provide the best description of epidemic pattern formation.

With regards to the model of interest, we considered the stochastic SIR model with long range interaction, as seen in example Ref. [18]; in this model the disease can transmit according to distance, *r*, in a power law distribution [20]. Therefore, the spread of the disease is essentially dependent on two main parameters: 1) The pathogenic ratio, which describes the ability of an organism, a pathogen, to produce an infectious disease in another organism; and 2) The pathogen level, which depends on the type of organism, e.g. influenza virus [21], HIV virus [22], and fungi [23].

II. Model And Simulation

A. Model

The pattern formation for epidemic spreading was studied by using Monte Carlo (MC) simulations. We considered a square lattice *L*x*L*, which for each site can be either empty or occupied by two types of individuals. The empty site represents a susceptible individual (*S*). The occupied particles are either infected (*I*) or immune (*R*) individuals. Therefore, the three state models are: *S*, *I*, and *R*, respectively.

For simplicity and without the loss of generality, we began by placing the infected or *I* individual at the origin and otherwise empty sites (susceptible or *S* individual) in the square lattice. To incorporate the disease transmission dynamics, *S* individuals were chosen randomly and converted into an *I* individual with probability αP, or to *R* with probability $(1-\alpha)P$, as schematically shown below:

$$S \xrightarrow{\alpha P} I$$

$$S \xrightarrow{(1-\alpha)P} R$$

where α is the pathogenic ratio and P is the total infected probability. The pathogenic ratio represents the pathogenicity of the virus or bacteria of interest. The spreading system that has the highest value of pathogenic ratio (α=1) corresponds to the spreading system, which doesn't have *R* individuals, and where the *S* individuals that have contact with infected individuals can change to only infected individuals. The spreading system that has the lowest value of pathogenic ratio (α=0) is the spreading system where the disease can not spread within the system because the *S* individuals that are in contact with infected individuals can only change to *I* individuals. The pathogenic ratio also describes how easily *S* individuals can be infected by the sick population.

Since the model that we are using is a long-range correlation, each *S* individual can be infected from any *I* individual. We let event A_i be an event that a given *S* individual is infected from the i^{th} *I* individual. So the total probability that a given *S* individual will be infected from any *I* individual is the probability of the union of all A_i events, $P(\bigcup_{i=1}^{N} A_i)$, where *N* is the total number of *I* individuals—since the infected event A_i is an independent event, i.e.

$$P(A_m \cap A_n) = P(A_m)P(A_n) \tag{1}$$

for any independent event A_m and A_n, and from the fact that

$$\begin{aligned} P(\bigcup_{i=1}^{N} A_i) &= \sum_{i=1}^{N} P(A_i) - \sum_{1\le k<j\le N} P(A_k \cap A_j) + \\ &\sum_{1\le k<j<i\le N} P(A_k \cap A_j \cap A_i) \\ &+\cdots-(-1)^N P(A_1 \cap A_2 \cap \cdots \cap A_N), \end{aligned} \tag{2}$$

Substituting eq. (1) in eq. (2), we then obtain

$$\begin{aligned} P(\bigcup_{i=1}^{N} A_i) &= P(A_1) + (1-P(A_1))P(A_2) + \cdots \\ &+(1-P(A_1))(1-P(A_2))P(A_3) + \cdots \\ &+\big(1-P(A_1)\big)(1-P(A_2))\cdots(1-P(A_{N-1}))P(A_N). \end{aligned} \tag{3}$$

Eq. (3) thus can be rearranged and becomes

$$P(\bigcup_{i=1}^{N} A_i) = 1 - \prod_{i=1}^{N} (1-P(A_i)) \cdot \tag{4}$$

Accordingly the total infected probability *P* is

$$\begin{aligned} P &= p_1 + (1-p_1)p_2 + (1-p_1)(1-p_2)p_3 + \ldots \\ &+\big(1-p_1\big)(1-p_2)\ldots(1-p_{N-1})p_N \\ &= 1 - \prod_{i=1}^{N} (1-p_i), \end{aligned} \tag{5}$$

where *N* is the number of *I* individuals in existence—see also ref. [18, 24]—and where p_i is the infected probability from the i^{th} *I* individual. Note that the probability formulae given in eq. (5) is used to find the total probability of many multi-event

problems; for example, the risk of infection of the total dose of infectivity in which each dose acts independently [25] and can be used to find the probability of *Trypanosoma cruzi* transmission to opossums by independent events of predation [26].

To incorporate the dynamics of how each type of population changes over time and what are the subsequent spatial pattern formations, in this model we let an *S* individual be infected by the i^{th} *I* individual, where the correlation probability p_i is expressed with long-range correlation [18, 27], which decays algebraically with the distance r_i. A flow chart of the simulation is shown in Fig. 1. We randomly chose an empty site located within a radius *L*/2 of a chosen infected individual such that the probability of infection by the i^{th} *I*

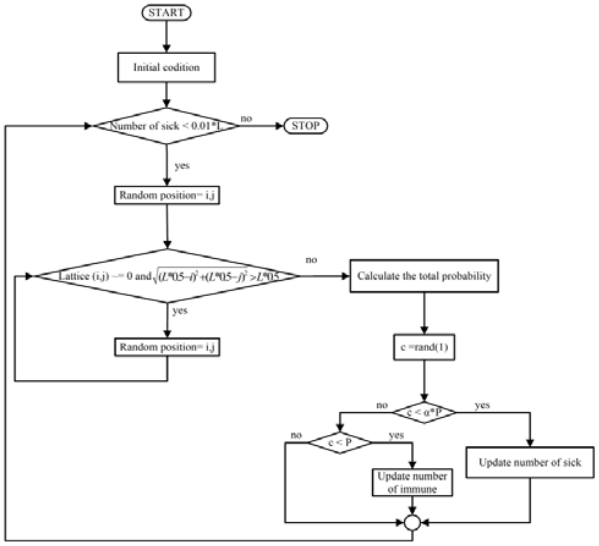

Fig. 1 shows the simulation diagram of epidemic spreading

individual is p_i, and the uninfected probability is 1-p_i. The correlation probability p_i as a power law probability is:

$$p_i = \frac{1}{r_i^{\beta}}, \tag{6}$$

where r_i is the distance from the chosen empty site to the i^{th} *I* site and β ($\beta \geq 0$) is the correlation exponent that relates to the way viruses spread and represents the correlation between individuals.

B. Measurements and characterization

To analyze spatial patterns, we measured four parameters: perimeter, circularity, fractal dimension, and aggregation index to investigate epidemic spreading.

Circularity is frequently included as a pattern formation in diverse formation analysis processes, and it has been used as the main property to evaluate morphological change in biological entities. The circularity measurement of a region (sometimes called the compactness) is used to measure the perimeter and the area of region and compute the following formula [28]:

$$C_{region} = \frac{4\pi \cdot Area}{Perimeter^2}. \tag{7}$$

Circularity equal to 1.0 denotes a perfect circle. As the value approaches 0.0, it indicates an increasingly elongated shape. This measure is independent of scale, as both nominator and denominator are proportional to the square of the perimeter for a given shape. A perimeter is a path that surrounds an area. Computationally, we used ImageJ software version 1.41o (http://rsb.info.nih.gov/ij/) to measure the circularity and perimeter.

For fractal dimension, we used the box-counting method, which was used by Hamburger *et al* to study a random set in a box. [29]. For a low occupied fraction, the apparent fractal behavior is observed between physically relevant cutoffs. The lower cutoff r_o is given by the length of particles (r_o=d), while the upper cutoff r_1 is given by the average gap between adjacent particles (r_1=$\rho^{-1/2}$-d) where ρ is the population density [17, 29]. In this study we used the commercial software Benoit 1.3 [16], which is specifically designed to analyze fractal dimension. In Benoit software, the fractal dimension is defined as the exponent D_f, where the relation is:

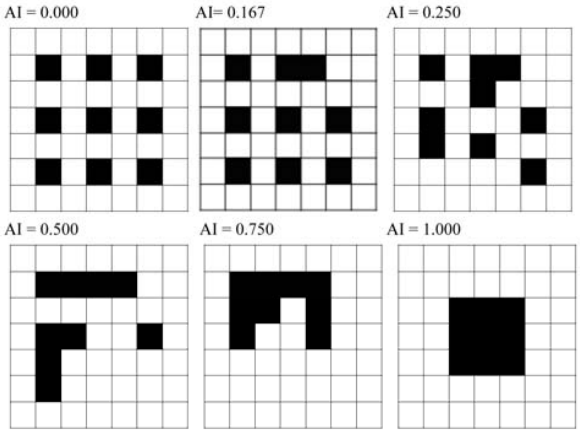

Fig. 2 shows the baseline of *AI* values ranging from 0 to 1

$$D_f = -slope\{\log r, \log N(r)\}. \tag{8}$$

As to the aggregation index (*AI*), it quantifies aggregation levels within a single class. An *AI* value is class specific and independent of landscape composition. Therefore the *AI* index can be used to quantify the level of aggregation of spatial patterns [15]. The highest level of aggregation (*AI* = 1) is comprised of pixels that share the most possible edges, whereas the lowest level of aggregation (*AI* = 0) is comprised of pixels that do not share edges. An *AI* was designed wherein landscapes were divided into a square grid. If $e_{i,j}$ represents the total edges of class *i* adjacent to class *j*, and $e_{i,i}$ is the total edges shared by class *i* itself, the actual level of the aggregation index of class *i* is defined as:

$$AI_i = \frac{e_{i,i}}{\max\_e_{i,i}}, \tag{9}$$

with max_$e_{i,i}$ being the largest number of possible edges

shared for class i. The value of $e_{i,i}$ is also known as the 'contact perimeter' [30]. The calculation of max_$e_{i,i}$ is based on the largest square integer n^2, which is smaller than the area A_i of class i. The AI values under various levels of aggregation are shown in Fig. 2. The binary landscapes are used with 0 for the background class (white) and 1 for class 1 (black). In this study, we used IAN: Image Analyzer version 1.0.16 software to find the values of the AI for a spreading pattern of population on a square lattice [15].

III. Results And Discussion

To study the spatial spread of the disease in a population where the spread of the infection is around a point source of infection, we firstly analyzed the distribution of I and R populations on the square lattice site L=500. The occupied fraction is, unless otherwise stated, 0.003= $N/\pi L^2$. We studied various pattern formations by varying the pathogenic ratio (α) and correlation exponent (β) of the long-range correlation model. We can classify the pattern of the $I\&R$ population into 3 formations as shown in Fig. 3: a) When the pattern exhibits spreading over a space lattice (no-clustering) for $\beta \in [0,2)$, b) When the pattern features clustering but not very packed (semi-cluster) for $\beta \in [2,5)$, and c) When the pattern is highly clustered and pack centered at the origin for $\beta \in [5,10]$. In the case of the small β ($\beta \in [0,2)$), the correlation between individuals is small or weak. The $I\&R$ population can spread randomly on the 2D lattice, as was expected and is shown in Fig. 3, β=0.5. As β increases there is, correspondingly, a stronger correlation; and when β is large enough (β>5), the correlation becomes very strong and the population can no longer spread randomly any more. The dispersed distributed pattern will thus change into partially dense patterns, where the population can only grow on the neighbor sites, leading to a cluster population. The compact clusters associated with a large (β>5) seem to be a self-affine front [1]. Moreover, the density of R population decreases as α increases. It should be pointed out though that these results are still qualitative. More quantitative analysis is needed and is discussed as follows.

To quantify the spatial structure of disease spread in a spatially distributed population density of I, R, and $I\&R$ population, we integrated the population density in radius r with $\Delta r = 10$, as shown in Fig. 4, by varying α = 0.4, 0.6, 0.8, and 1.0 and β = 0.5, 3.00, and 7.50. These measures describe how the density of the surrounding population varies as a function of the distance from the origin.

Each figure represents three population densities: I, R, and $I\&R$ population, respectively. In Fig. 4 (1st column), the populations become more homogenous as the radius increases. This indicates that the population can spread uniformly and randomly from the center of the lattice system. It was observed that for small β (or weak correlation), I population radial structures are barely distinguishable even when α increases, while the means of R and $I\&R$ population density increase. However, the distinction between I population radial structures when α values are different is more pronounced when β is large enough. These results imply that for the weak correlation α does not affect pattern formation. For the analysis of the curve in Fig. 4 (2nd column), we tried to fit the curves with the Lorentz function [31]:

$$y(x) = y_0 + \frac{2A}{\pi}\left[\frac{W}{4(x-x_c)^2 + W^2}\right], \tag{10}$$

where x_c is the mean value, W is the full width at half maximum, and A is the area under the graph. The fitting parameters are shown in table 1 and correspond to Fig. 4 (2nd column). For I population density, the population densities with radii = 10 to 30 increase as α increases, while the R population densities decrease. The explanation for this is that since the probability $(1-\alpha)P$ is lower when α is greater, it results in a decrease in the number of S individuals eventually becoming R individuals. These results are consistent with those given in Fig. 3.

For of the case of large β=7.5 (see Fig. 4 (3rd column)), we found that the population densities may be described by the Gaussian function

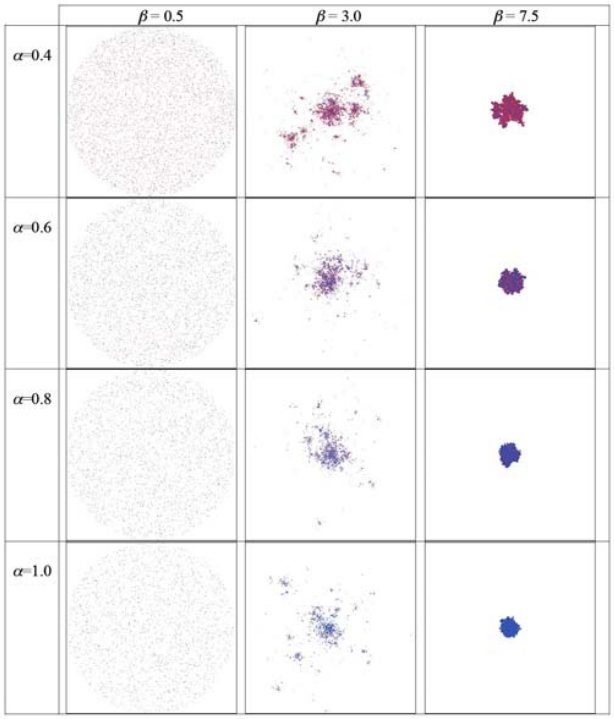

Fig. 3 shows the pattern spreading of long-range correlation of the $I\&R$ population. White area, Blue spot, and Red spot represent S, I, and R individuals, respectively where α = 0.4, 0.6, 0.8, and 1.0 and β = 0.5, 3.0, and 7.5

$$y(x) = y_0 + \frac{A}{\sqrt{2\pi}\sigma}\exp\left[-\frac{(x-x_c)^2}{2\sigma^2}\right], \tag{11}$$

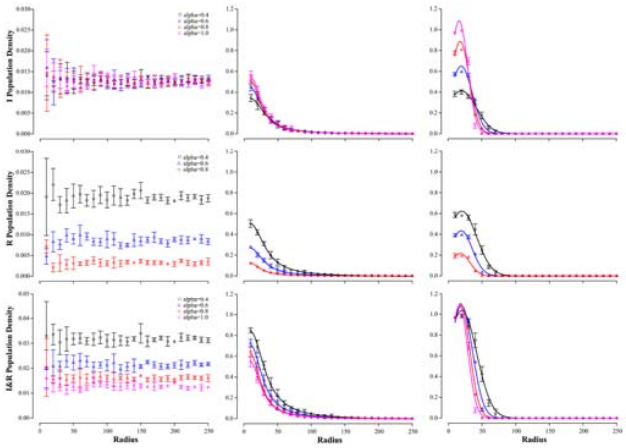

Fig. 4 show the density of *I* (upper), *R* (middle), and *I*&*R* (lower) population that integrate with dr= 10 where r is radius from the center with vary α = 0.4 (○), 0.6 (△), 0.8 (□), and 1.0 (◇) and β = 0.5(1st column), β = 3.0(2nd column) with the fitting Lorentz function

TABLE I
THE FITTING PARAMETERS OF LORENTZ FUNCTION

α	0.4			0.6		
	I	R	I&R	I	R	I&R
y_0	-0.0043	-0.0073	-0.0116	-0.0033	-0.0032	-0.0064
x_c(mean)	10.00	10.00	10.00	10.00	10.00	10.00
W(width)	48.14	48.97	48.65	38386	43.31	40.49
A(area)	25.80	39.18	64.99	27.13	18.42	45.48
H(height)	0.34	0.51	0.84	0.44	0.27	0.71
R-square	0.998	0.998	0.998	0.999	0.994	0.999

α	0.8			1.0		
	I	R	I&R	I	R	I&R
y_0	-0.0017	-0.0005	-0.0022	-0.0057		-0.0060
x_c(mean)	10.00	10.00	10.00	10.00		10.00
W(width)	34.08	34.75	34.21	36.79		36.85
A(area)	27.12	6.65	33.77	31.64		31.70
H(height)	0.50	0.12	0.63	0.54		0.54
R-square	0.995	0.998	0.995	0.998		0.997

where x_c is the median of curve and σ is the standard deviation. These parameters are shown in table 2. From further curves analysis; it was found that the variations characterized by σ decrease when α increases. Note that 2σ is the width of fitting curve. When considering *I* and *I*&*R* population densities, we found that 2σ values decrease when α values increase from 0.40 to 1.00. These findings reflect that the spatial patterns tend to be more packed or clustered for high pathogenic ratio scenarios. Furthermore, when we compared the results of *I* population densities of β between 3.0 and 7.5, it was found that the higher correlation of the epidemic spread drives the spatial pattern to become more packed. So far, it can be seen that when pathogens are very easily spread (which corresponds to the weak correlation case), the disease can be transmitted long distances, while the distribution of *I* and *R* individuals are dispersed. This situation could correspond to a disease spread that is mediated by such things as wind, air travel [32], or the migration of birds [33]. In contrast, when diseases can only spread at short range, this situation may be related to a strong correlation spread. The corresponding epidemics for these cases are mainly those which are transmitted by surface contact, body fluids, or sexual contact [34].

A. Perimeter and Circularity

To characterize the dynamic of the spatial pattern, we used perimeter, circularity, fractal dimension, and the aggregation index to analyze the distribution population on a square lattice site L=500. In those cases where there was the strong correlation β=10 (for the clustered patterns) and α varied from 0.3 to 1.0, Fig. 5 shows the *R*/*I* ratio of the population, the perimeter, and the circularity, respectively. With regards to the *R*/*I* ratio of the population, it was found that this ratio decreases as α increases. The perimeter, which is a length that surrounds a cluster or the circumference of a pattern, also decreases as α increases from 0.3 to 0.7 for the *I* and *I*&*R* populations. This implies that the pattern formation tends to be more clustered or packed as α gets larger. For α<0.6, the perimeter of the *I* population is greater than the *I*&*R* population. This is because the clusters of the *I* population consist of many small clusters which can spread out over a very long distance. Generally, a larger perimeter implies that it is difficult to prevent the epidemic from spreading and limit transmission to a finite control range or endemic limit. When compared with the lower perimeter value, the spreading pattern is more clustered to a finite site although the α value is small. For this situation it is not difficult to control the disease spread. For the perimeter of *R* population, the results show it increases as α is higher until about α =0.6, because once again the total probability (1-α)*P* is smaller. Consequently, a lesser number of *S* individuals become *R* individuals, which results in small clusters.

For the circularity results, which relates to the roundness of the spreading pattern, we can divide the curve into two parts like a perimeter measure. The circularity increases when we increase α in the range 0.3-0.6. For α>0.6, the circularity becomes steady at about the value of 0.25. It can be seen that the circularity values are very low for α = 0.3-0.7 and seldom for α>0.7, implying that the patterns are not a perfect circle and that the disease cannot spread in the same radius from the center. These results indicate that the epidemic spread cannot

TABLE II
THE FITTING PARAMETERS OF GAUSSIAN FUNCTION

α	0.4			0.6		
	I	R	I&R	I	R	I&R
y_0	0	0	0	0	0	0
x_c(mean)	20.07	20.05	20.06	19.58	18.99	19.34
σ (std.)	22.07	21.86	21.95	16.21	16.33	16.26
A(area)	22.85	34.17	57.02	26.44	17.79	44.23
H(height)	0.41	0.62	1.036	0.65	0.43	1.08
R-square	0.995	0.995	0.995	0.987	0.987	0.987

α	0.8			1.0		
	I	R	I&R	I	R	I&R
y_0	0	0	0	0		0
x_c(mean)	18.00	17.91	17.98	16.94		16.49
σ (std.)	13.54	13.98	13.63	12.33		12.33
A(area)	30.17	7.58	37.76	33.71		33.71
H(height)	0.89	0.22	1.10	1.09		1.09
R-square	0.985	0.985	0.985	0.988		0.988

spread to infinite for the strong correlation; therefore the cluster of epidemic spreading is on the finite scale, and it can see that α plays an important role in the spread of the disease.

B. Fractal Dimension

To analyze the dynamic process of I population spreading, we used the fractal dimension to express the geometric properties. The fractal dimension (D_f) of a spreading epidemic can be calculated by the box-counting method [29], as shown

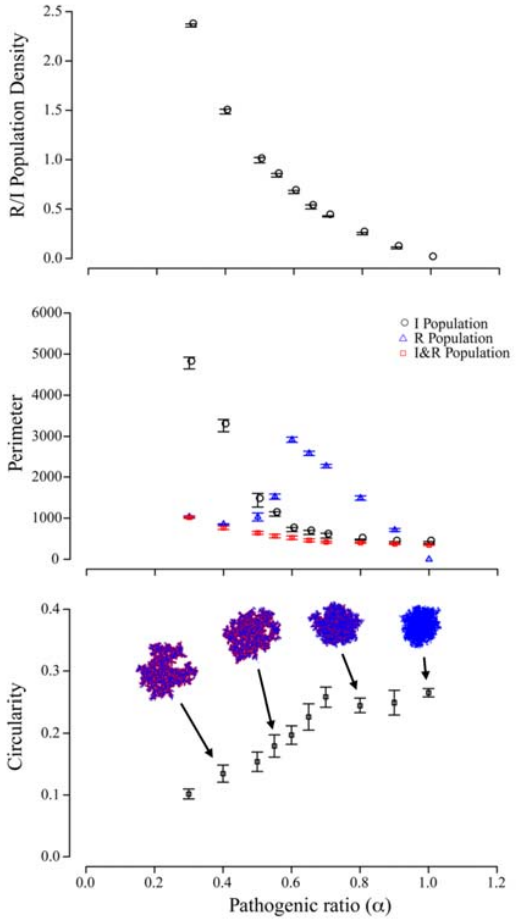

Fig. 5 show the R/I ratio of population (upper), the perimeter of I (○) and $I\&R$ (△) population (middle), and the circularity (lower) of the cluster of $I+R$ population as α increases from 0.3 to1.0 for the β = 10.00

D_f is a quantity that gives information as to how completely a spatial representation appears to fill space [35]. D_f also provides a measure of the degree of correlation between individuals over space and is used to analyze fragmented spatial phenomena in terms of self-similarity or self-affine. From this result, it was found that the D_f value increases from 0.71 to 1.84 when β increases. And it has a transition pattern at $\beta \approx 2$. This result agrees with the previous work of Tan and co-workers [18, 19]. They showed that when β rises from 0 to infinite, the fractal dimension sharp step appears at $\beta \approx 2$. The small value D_f (0.71) relates to the occupied fraction [29]. As to percolation space, it seems that site percolation occurs for any α [36]. This implies that at each step of simulation, the pattern formation grows with weak correlation ($0<\beta<2$), and that the I population can disperse randomly in percolation space.

When the D_f value increases the pattern formation changes to Leath percolation [37]. Leath percolation is useful for studying the structure of percolation clusters. The pattern formation here is more packed and grows from the nearest neighbor of the initial site. Because between individuals there exists a strong correlation ($\beta>5$), they can grow in a short-range correlation. When $\beta \to \infty$, the D_f value approaches 2 and

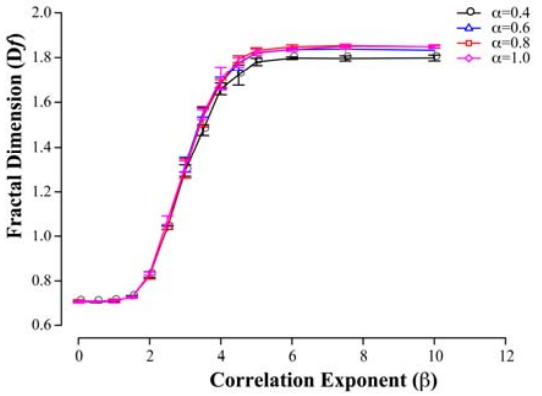

Fig. 6 show the fractal dimension (D_f) of the cluster I population as the β increase from 0.01 to 10.00 for epidemic spreading with vary α from 0.4 to 1.0

the dynamics reduces to the Eden model [1, 38], which is just the growth rule of dense cluster growth. However, it was found that D_f cannot be used to discriminate or indicate the pattern dynamics for any α when $\beta>5$. This result shows the limitation of considering pattern formations when varying α. This measurement can describe the dynamic pattern for just the β parameter. The α parameter though is important to epidemic spreading because disease epidemics have difference pathogenic levels, which impacts the speed and violence of an epidemic's spread.

C. Aggregation Index

From the previous results, we used the aggregation index to describe the pattern dynamics of I population spreading calculated by IAN software [15]. The AI measurement provides a quantitative basis from which to correlate spatial patterns with processes that are typically class specific. We found that when the correlation exponent rises from 0 to 10, AI increases from 0 to 0.9, and the sharp step appears at $\beta=2$, as seen in Fig. 7. These findings show the likely results of the fractal dimension method for varying α and β, which has a transition pattern at $\beta \approx 2$.

We can divide the graph into 3 parts. In the first part the correlation exponent is less than 2. It was found that the AI did not change and was close to 0. This shows the result of the weak correlation between individuals and agrees with the previous results. The I individuals can spread randomly in 2D space, and they don't have adjacent neighbors. The second part (for $2<\beta<5$) shows the pattern transition, where the AI value increases when β increases for every range of α. The

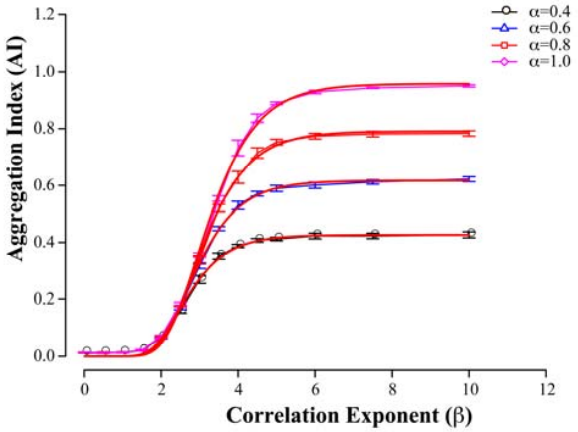

Fig. 7 show the aggregation index (*AI*) of the cluster *I* population as the β increase from 0.01 to 10.00 for epidemic spreading with vary α from 0.4 to 1.0 and show the fitting curve with Gompertz function.

TABLE III
THE FITTING PARAMETERS OF GOMPERTZ FUNCTION

α	0.4	0.6	0.8	1.0
b	0.427	0.617	0.791	0.956
x_c(mean)	2.455	2.665	2.821	2.945
k	1.454	1.335	1.258	1.187
R-square	0.998	0.998	0.998	0.998

final part (β>5) shows the stationary pattern, where the *AI* value becomes steady. When α increases, the probability that *S* individuals changing to *R* individuals ((1-α)*P*) decreases, so the *S* neighbors of pattern are more likely to change to *I* individuals and results in the increasing of *AI*. The epidemic spreading becomes clustered with a difference level that corresponds to α. It was found that the *AI* measurement can be used to distinguish the level of various α values that are different for the fractal dimension measurement [18]. This result could be well-fitted to the Gompertz function [39]

$$y = be^{-\exp -k(x-x_c)}. \quad (11)$$

These fitting parameters are shown in table 5, where -*k* is the rate of clustering and x_c is the mean of the x parameter. Here *b* is the maximum value that can be reached with the $\beta \to \infty$ and

$$\lim_{\beta \to \infty} AI(\beta) = b. \quad (12)$$

From the fitting results, we found that the *b* values can be fitted with the pathogenic ratio as shown in table 3. Therefore, the *AI* parameters can reflect the α values when β>5. The α value is important in describing the virulence of bacteria or the virus that causes disease and the virulence of its spread. At low pathogenicity (e.g. influenza), a virus or bacteria usually causes only mild or undetected symptoms, but at high pathogenicity, they may spread more rapidly though intermediaries, as occurs with avian flu, SARS, dengue, and so no. Moreover, the *AI* results indicate the probability of having an adjacent neighbor and imply the possibility of infection among individuals. For the *k* parameter results, it was found that the high α has a greater rate of clustering when compared with the low α. None of these results can be obtained through previous methods, especially in terms of the fractal dimension.

IV. CONCLUDING REMARKS

Using the epidemic model with long-range correlation, we show the spatial pattern of a spreading epidemic and analyze it using the perimeter, circularity, fractal dimension, and aggregation index methods. The perimeter of the *I*, *R*, and *I*+*R* population and the circularity of *I*+*R* population describe the size and symmetric direction of the spreading pattern only for β=10. The fractal dimension describes only the growth rule of pattern formation in the *I* population with variable α and β parameters. However these methods cannot describe and distinguish the dynamics of the pathogenic level when β>5. To characterize the pathogenic ratio, we thus use the aggregation index method as an alternative method. Moreover, this method indicates the α parameter when β>5. This is the parameter used to describe the virulence of disease spreading.

ACKNOWLEDGMENT

The authors thank Mr. David Blyler for editing the manuscript and providing comments. We would like to thank the Commission on Higher Education Thailand for its grant support under the Strategic Scholarships for Frontier Research Network for joint Ph.D. Programs. This research project is supported by Faculty of Science, Mahidol University, the Thailand Research Fund (TRF), the Commission on Higher Education, Ministry of Education, Mahidol University Research Grant, Center of Excellence for Innovation in Chemistry (PERCH-CIC), and and The Thailand Center of Excellence in Physics (ThEP).

REFERENCES

[1] A.-L. Barabási, H.E. Stanley, Fractal Concepts in Surface Growth, Cambridge University Press, Cambridge, 1995.
[2] J. Northcott, M.C. Andersen, G.W. Roemer, E.L. Fredrickson, M. Demers, J. Truett, P.L. Ford, Spatial Analysis of Effects of Mowing and Burning on Colony Expansion in Reintroduced Black-Tailed Prairie Dog, Restor. Ecol. 16, 495-502, 2008.
[3] J. Meliker, G. Jacquez, P. Goovaerts, G. Copeland, M. Yassine, Spatial cluster analysis of early stage breast cancer: a method for public health practice using cancer registry data, Cancer Cause Control 20, 1061-1069, 2009.
[4] R. Schlicht, Y. Iwasa, Spatial pattern analysis in forest dynamics: deviation from power law and direction of regeneration waves. Ecol. Res. 22, 197-203, 2007.
[5] G. Sun, Z. Jin, Q. Liu, L. Li, Pattern formation in a spatial SI model with non-linear incidence rates, J. Stat. Mech. 11, 11011, 2007.
[6] Q. Liu, Z. Jin, Formation of spatial patterns in an epidemic model with constant removal rate of the infectives, J. Stat. Mech. 5002, 2007.
[7] D. Eisinger, H. Thulke, Spatial pattern formation facilitates eradication of infectious diseases, J. Appl. Ecol. 45, 415-423, 2008.
[8] Z. Qiu, Dynamical behavior of a vector-host epidemic model with demographic structure, Comput. Math. Appl. 56, 3118-3129, 2008.
[9] F. Santos, J. Rodrigues, J. Pacheco, Epidemic spreading and cooperation dynamics on homogeneous small-world networks, Phys. Rev. E 72, 56128, 2005.
[10] U. Kitron, Landscape ecology and epidemiology of vector-borne diseases: tools for spatial analysis, J. Med. Entomol. 35, 435-445, 1998.
[11] L. Cobb, Stochastic differential equations for the social sciences, Mathematical frontiers of the social and policy sciences, 37–68, 1981.

[12] J. Ma, Q.-M. Zhao, Circular pattern extraction in wafer fault mining, International Conference on Wavelet Analysis and Pattern Recognition, Hong Kong, 123-127, 2008.
[13] J. Žunić, K. Hirota, Measuring Shape Circularity, in: J. Ruiz-Shulcloper, W.G. Kropatsch (Eds.), Progress in Pattern Recognition, Image Analysis and Applications, Springer Berlin, Heidelberg, 94-101, 2008.
[14] U. Purintrapiban, V. Kachitvichyanukul, Detecting patterns in process data with fractal dimension, Comput. Ind. Eng. 45, 653-667, 2003.
[15] H.S. He, B.E. DeZonia, D.J. Mladenoff, An aggregation index (AI) to quantify spatial patterns of landscapes, Landscape Ecol. 15, 591-601, 2000.
[16] C.M. Hagerhall, T. Purcell, R. Taylor, Fractal dimension of landscape silhouette outlines as a predictor of landscape preference, J. Environ. Psychol. 24, 247-255, 2004.
[17] O. Biham, O. Malcai, D.A. Lidar, D. Avnir, Pattern formation and a clustering transition in power-law sequential adsorption, Phys. Rev. E 59, R4713, 1999.
[18] Z.-J. Tan, X.-W. Zou, Z.-Z. Jin, Percolation with long-range correlations for epidemic spreading, Phys. Rev. E 62, 8409, 2000.
[19] Z.-J. Tan, C. Long, X.-W. Zou, W. Zhang, Z.-Z. Jin, Epidemic spreading in percolation worlds, Phys Lett. A 300, 317-323, 2002.
[20] J. Adamek, M. Keller, A. Senftleben, H. Hinrichsen, Epidemic spreading with long-range infections and incubation times, J. Stat. Mech-Theory E., 09002, 2005.
[21] J.A. van der Goot, G. Koch, M.C. de Jong, M. van Boven, Quantification of the effect of vaccination on transmission of avian influenza (H7N7) in chickens, P. Natl. Acad. Sci. USA 102, 18141-18146, 2005.
[22] F. Wang, Z. Ma, Y. Shag, A competition model of HIV with recombination effect. Math. Comput. Model. 38, 1051-1065, 2003.
[23] F. Stagnitti, A model of the effects of nonuniform soil-water distribution on the subsurface migration of bacteria: Implications for land disposal of sewage, Math. Comput. Model. 29, 41-52, 1999.
[24] R.M. Weseloh, Short and Long Range Dispersal in the Gypsy moth (Lepidoptera: Lymantriidae) Fungal Pathogen, Entomophaga maimaiga (Zygomycetes: Entomophthorales), Environ. Entomol. 32, 111-122, 2003.
[25] M.B. Gravenor, N. Stallard, R. Curnow, A.R. McLean, Repeated challenge with prion disease: the risk of infection and impact on incubation period, P. Natl. Acad. Sci. USA 100, 10960-10965, 2003.
[26] J. Rabinovich, N. Schweigmann, V. Yohai, C. Wisnivesky-Colli, Probability of *Trypanosoma cruzi* transmission by Triatoma infestans (Hemiptera: Reduviidae) to the opossum Didelphis albiventris (Marsupialia: Didelphidae), Am. J. Trop. Med. Hyg. 65, 125-130, 2001.
[27] F. Ginelli, H. Hinrichsen, R. Livi, D. Mukamel, A. Torcini, Contact processes with long range interactions, J. Stat. Mech., 08008, 2006.
[28] J. Kilday, F. Palmieri, M.D. Fox, Classifying mammographic lesions using computerized image analysis, IEEE Trans. Med. Imaging 12, 664-669, 1993.
[29] D. Hamburger, O. Biham, D. Avnir, Apparent fractality emerging from models of random distributions, Phys. Rev. E 53, 3342-3358, 1996.
[30] E. Bribiesca, Measuring 2-D shape compactness using the contact perimeter, Comput. Math. Appl. 33, 1-9, 1997.
[31] K. Shanmugan, A. Breipohl, Random signals: detection, estimation, and data analysis, John Wiley & Sons Inc, 1988.
[32] J. Lessler, J.H. Kaufman, D.A. Ford, J.V. Douglas, The cost of simplifying air travel when modeling disease spread, PLoS ONE 4, 4403, 2009.
[33] K.D. Reed, J.K. Meece, J.S. Henkel, S.K. Shukla, Birds, migration and emerging zoonoses: west nile virus, lyme disease, influenza A and enteropathogens, Clin Med. Res. 1, 5-12, 2003.
[34] M. Bohm, K.L. Palphramand, G. Newton-Cross, M.R. Hutchings, P.C.L. White, Dynamic interactions among badgers: implications for sociality and disease transmission, J. Anim. Ecol. 77, 735-745, 2008.
[35] M.F.M. Lima, J.A. Tenreiro Machado, M. Crisostomo, Filtering method in backlash phenomena analysis, Math. Comput. Model. 49, 1494-1503, 2009.
[36] D. Stauffer, A. Aharony, Introduction to percolation theory, Taylor & Francis, London, 2003.
[37] P.L. Leath, Cluster size and boundary distribution near percolation threshold, Phys. Rev. B 14, 5046-5055, 1976.
[38] P. Meakin, Fractals, Scaling and Growth Far From Equilibrium, Cambridge University Press, Cambridge, 1998.
[39] B. Gompertz, On the nature of the function expressive of the law of human mortality and on a new mode of determining life contin-gencies, Philos. Trans. R. Soc. Lond. 115, 513-585, 1825.